ARTICLE IN PRESS

Catalysis Today xxx (xxxx) xxx–xxx

Contents lists available at ScienceDirect

Catalysis Today

journal homepage: www.elsevier.com/locate/cattod

Photocatalytic degradation of phenolic pollutants using *N*-methylquinolinium and 9-mesityl-10-methylacridinium salts

R. Martinez-Haya, M.M. Luna, A. Hijarro, E. Martinez-Valero, M.A. Miranda*, M.L. Marin*

Instituto de Tecnología Química, Universitat Politècnica de València-Consejo Superior de Investigaciones Científicas, Avda. de los Naranjos s/n, E-46022, Valencia, Spain

ARTICLE INFO

Keywords:
Electron transfer
Photocatalysis
Singlet excited state
Steady-state fluorescence
Time-resolved fluorescence

ABSTRACT

The photodegradation of a mixture of phenolic pollutants including: phenol (P), *orto*-phenylphenol (OPP), 2,4,6-trichlorophenol (TCP) and pentachlorophenol (PCP) was accomplished using two organic cationic photocatalysts, namely *N*-methylquinolinium (NMQ^+) and 9-mesityl-10-methylacridinium ($Mes\text{-}Acr\text{-}Me^+$) salts, due to their singular photophysical and redox properties. On one hand, NMQ^+ exhibits more energetic excited states and accordingly more favorable redox potentials than $Mes\text{-}Acr\text{-}Me^+$; on the other hand, NMQ^+ absorption reaches only up to 380 nm, while $Mes\text{-}Acr\text{-}Me^+$ extends in the visible up to 480 nm. Evaluation of the efficiency of both photocatalysts, revealed that the highest level of photodegradation was achieved when they were employed at 20% mol. Specifically, with NMQ^+, removal of the pollutants was completed within 24 h of irradiation. Even more, irradiation time could be shortened from 24 to 8 h, since high levels of removal were already achieved (93%, 100%, 100% and 82% for P, OPP, TCP and PCP, respectively). Albeit, $Mes\text{-}Acr\text{-}Me^+$ was not as effective, and best results were obtained using 20% mol upon 24 h of irradiation. Under these conditions, removal of PCP was 80%, while TCP was 40%, OPP 30% and P resulted in the most recalcitrant contaminant with only 10% of removal. Next, NMQ^+ and $Mes\text{-}Acr\text{-}Me^+$ were separately supported onto Zeolite Y, an inert inorganic support ($Y\text{-}NMQ^+$ and $Y\text{-}Mes\text{-}Acr\text{-}Me^+$), and elemental analyses revealed a loading of *ca.* 13% and 15% weight for NMQ^+ and $Mes\text{-}Acr\text{-}Me^+$, respectively. Upon heterogenization, in the case of $Y\text{-}NMQ^+$, the extent of removal was lower than the one achieved in the homogeneous photodegradations. On the contrary, performance of $Y\text{-}Mes\text{-}Acr\text{-}Me^+$ improved, because of its enhanced photostability; thus, upon 46 h irradiation, 98%, 80%, 40% and 26% for PCP, TCP, OPP and P, respectively, was achieved. Moreover, their efficiency was maintained upon second use. Steady-state and time-resolved fluorescence quenching revealed that every pollutant was able to quench the singlet excited state of both $^1(NMQ^+)^*$ and $^1(Mes\text{-}Acr\text{-}Me^+)^*$, with kinetic rate constants in the order of the diffusion limit. Thus, Type I photooxidation happening through the singlet excited state of either photocatalyst was the main operating process in the photodegradation of the studied pollutants.

1. Introduction

Extensive agriculture is currently a motor of the economy for many countries; however, it is accompanied with several environmental problems such as massive use of pesticides, spoiled soils or use of huge volumes of water. In the Mediterranean area, production of olives accounts for approximately 63% of world production [1]. However, one of the main drawbacks associated with this industry is the great amount of wastewaters generated by olive oil production [2]. These wastewaters contain high concentrations of phenolic compounds, lipids, sugars and polyphenols [3]; therefore, they require specific pretreatments to prevent serious problems in the usual biological treatment processes.

Special attention has recently been paid to advanced oxidation processes (AOPs) to deal with the organic matter present in the wastewaters [4]. Among AOPs, photocatalysis constitutes an emerging green process with a proven potential for water remediation [5]. More specifically, organic photocatalysts offer the possibility of investigating the reaction mechanisms involved in photooxidation upon studying the reactivity of the photogenerated excited states by means of time-resolved techniques in the nano or micro-second scale [6].

With this background, the aim of the present work is to investigate the photodegradation of a mixture of phenolic pollutants (Fig. 1) including: phenol (P), *orto*-phenylphenol (OPP), 2,4,6-trichlorophenol (TCP) and pentachlorophenol (PCP). They are generated in agriculture due to the widespread use of antifungals or pesticides [7]. To achieve the photodegradation of this group of pollutants, herein we have

---

* Corresponding authors.
E-mail addresses: mmiranda@qim.upv.es (M.A. Miranda), marmarin@qim.upv.es (M.L. Marin).

https://doi.org/10.1016/j.cattod.2019.01.045
Received 14 July 2018; Received in revised form 5 January 2019; Accepted 15 January 2019

Please cite this article as: Martinez-Haya, R., Catalysis Today, https://doi.org/10.1016/j.cattod.2019.01.045

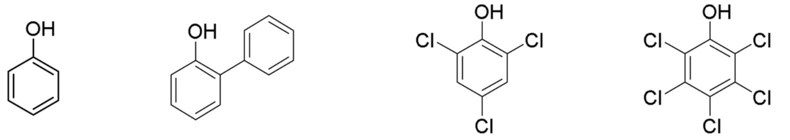

Phenol **(P)** | *orto*-Phenylphenol **(OPP)** | 2,4,6-Trichlorophenol **(TCP)** | Pentachlorophenol **(PCP)**

Fig. 1. Chemical structures of the selected pollutants.

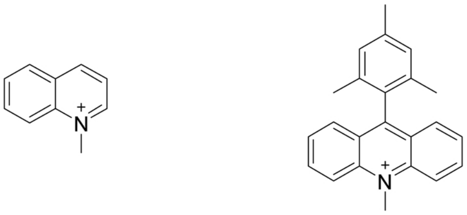

	N-methylquinolinium (**NMQ**$^+$)[6, 17]	9-Mesityl-10-methylacridinium (**Mes-Acr-Me**$^+$)[11]
E_{red} (V *vs* SCE)	-0.85	-0.49
E^*_S (eV)	3.55	2.67
E^*_T (eV)	2.65	1.94
τ_S (ns)	20	6.0^a
τ_T (μs)	-	30^b
Φ_Δ	0.85	0.21
Φ_F	0.85	0.21[9]
Φ_{isc}	<0.15	0.38[11]

Fig. 2. Chemical structures, redox and photophysical properties of NMQ$^+$ and Mes-Acr-Me$^+$. ^{a}Equilibrium between the locally excited and the charge transfer singlet species. ^{b}The triplet species could be assigned to the locally excited and/or the charge transfer species [9–11].

focused our attention on two organic cationic photocatalysts, namely *N*-methylquinolinium (NMQ$^+$) and 9-mesityl-10-methylacridinium (Mes-Acr-Me$^+$) salts [8], due to their singular photophysical and redox properties (Fig. 2) [9–11]. Among their potential advantages as photocatalysts, they do not contain metals and, being cationic, they should allow for efficient photoinduced electron transfer, due to the lack of Coulombic attraction between the resulting species. Moreover, although both cations can generate singlet oxygen, previous results from our group have demonstrated that the contribution of this reactive oxygen species for the overall oxidation at typical pollutant concentrations is negligible compared to the photoinduced electron transfer pathway at the typical pollutant concentration in water [12,13]. Even more, although these photocatalysts have attracted some attention in the recent years [9,12,14,15], to the best of our knowledge, neither Mes-Acr-Me$^+$ nor related acridinium salts have been employed in pollutants treatment.

In spite of the fact that NMQ$^+$ and Mes-Acr-Me$^+$ share several advantages, they have certain properties that make them different enough to deserve a deeper evaluation. For instance, NMQ$^+$ exhibits more energetic excited states than Mes-Acr-Me$^+$; this combined with the more favorable redox potential makes NMQ$^+$ more attractive as Type I photocatalyst (Fig. 2). Nevertheless, NMQ$^+$ absorption reaches only up to 380 nm, while Mes-Acr-Me$^+$ extends in the visible up to 480 nm (Figure S1). Whether one or the other parameter is more important would depend on the performance at the specific context and on the energetic and cost balances. Furthermore, while NMQ$^+$ must be synthesized, Mes-Acr-Me$^+$ is commercially available.

Therefore, photodegradation of the mixture of phenolic pollutants has been evaluated in parallel with the two photocatalysts. In addition, both NMQ$^+$ and Mes-Acr-Me$^+$, have been supported onto zeolite Y-100 to investigate the abatement of pollutants in heterogeneous phase. Finally, a detailed time-resolved photophysical study has been undertaken to elucidate the operating mechanism.

2. Experimental

2.1. Chemicals

Phenol, *orto*-phenylphenol, 2,4,6-trichlorophenol, pentachlorophenol, *p*-xylene and 9-mesityl-10-methylacridinium perchlorate were purchased from Sigma Aldrich. Zeolite Y 100 was obtained from Zeolyst International. Water used in electrochemical measurements and photodegradation experiments was Milli-Q grade; acetonitrile (ACN) was of HPLC quality from Scharlau and dimethyl sulfoxide (DMSO) was from Across. *N*-Methylquinolinium tetrafluoroborate salt was synthesized from quinoline (Sigma Aldrich) in two steps as previously described [16,17]. Briefly, quinoline (0.42 mol) and methyl iodide (0.64 mol, 1.5 eq) were heated at 65 °C, under reflux for 24 h; afterwards, the resulting solid crude (*N*-methylquinolinium iodide) was washed with ether (see spectroscopic details in Figure S2). The solid *N*-methylquinolinium iodide was treated with $BF_3{\cdot}Et_2O$ (1.1 mol, 2.6 eq) at 50 °C under stirring for 2.5 h, under nitrogen atmosphere. An additional amount of $BF_3{\cdot}Et_2O$ (1.1 mol) was added and the mixture was stirred for further 2.5 h. The resulting solid was washed with ether and recrystallized from ethanol to yield *N*-methylquinolinium tetrafluoroborate (see spectroscopic details in Figure S3).

Photocatalysts adsorption onto zeolite Y 100 was performed according to a previously described procedure [18]. Briefly, for the heterogeneization of NMQ^+ (Y-NMQ^+), Y-zeolite 100 (6.2 g) was suspended on an aqueous solution (25 mL) containing NMQ^+ tetrafluoroborate (1.0 g). The mixture was stirred at 40 °C for 24 h in the dark. Then, the solid was filtered, washed with water (30 mL) and dried at 100 °C for 72 h. Heterogeneization of Mes-Acr-Me^+ (Y-Mes-Acr-Me^+) was performed as follows [19]: Y-zeolite 100 (5 g) was suspended on a ACN:H_2O (1:1) solution (20 mL) containing Mes-Acr-Me^+ perchlorate (0.82 g). The mixture was stirred at 40 °C for 24 h in the dark. Then, the solid was filtered, washed with water (30 mL) and dried at 100 °C for 72 h. Loading of NMQ^+ and Mes-Acr-Me^+ on Y-NMQ^+ and Y-Mes-Acr-Me^+ were 13% wt and 15% wt, respectively, according to the elemental analysis.

2.2. Cyclic voltammetry

Cyclic voltammetric experiments were carried out using a cylindrical three-electrode quartz cell on a VersaSTAT 3 (Princeton Applied Research) electrochemical workstation with a glassy carbon (GCE) working electrode, a Pt wire counter electrode and a AgCl/Ag (sat KCl) as the reference electrode, in a one compartment electrochemical cell. The GCE and the Pt electrodes were polished using diamond spray (particle size 0.05 μm) before each experiment.

Pollutant stock solutions (1 mM) were prepared in mixtures H_2O:DMSO (24:1) for P, OPP and TCP, and in ACN for PCP. The cyclic voltammetries were carried out at room temperature, under a constant flux of N_2 using solutions of 30 μM of each pollutant in 0.1 M aqueous phosphate buffer pH 7 for P, OPP and TCP or in 0.1 M tetrabutyl ammonium perchlorate in ACN for PCP. The speed for the measurements was fixed at $0.05\ V{\cdot}s^{-1}$. The values of the redox potentials were calculated as the average between the maximum and minimum of the cyclic potential scan curves when the redox reactions were reversible, or from the maximum obtained in the voltammograms for the irreversible processes (Figure S4). The obtained data from the AgCl/Ag (sat KCl) were converted into redox potential values *vs* standard calomel electrode (SCE) as follows: E (*vs* SCE, in V) = E (*vs* AgCl/Ag, in V) -0.045 (Table S1).

2.3. Photocatalytic degradations

Homogeneous photochemical reactions were carried out in test tubes with magnetic stirring using a Luzchem photoreactor (model LZC-4 V) equipped with lamps emitting at 350 nm (9 bulbs, FL8BL-B model from Hitachi) or 420 nm (7 bulbs, LZC420 model from Luzchem Research Inc.), for NMQ^+ or Mes-Acr-Me^+, respectively. Aqueous solutions (9 mL) containing a mixture of the four pollutants (P, OPP, TCP and PCP, 5×10^{-5} M each, 2×10^{-4} M in total) were irradiated under air, in the presence of different photocatalyst ratios (NMQ^+ or Mes-Acr-Me^+ at 5, 10 or 20% mol, referred to the total pollutant concentration). The removal of the pollutants at different irradiation times was monitored by HPLC.

For the heterogeneous photoreactions, aqueous mixtures of 15 mL containing the four pollutants (5×10^{-5} M each) and the heterogeneous photocatalyst ($93\ mg\ L^{-1}$, 26% mol, for Y-NMQ^+ or $160\ mg\ L^{-1}$, 30% mol in the case of Y-Mes-Acr-Me^+), were stirred for 60 min in dark and then irradiated under air, using the above described Luzchem photoreactor. Aliquots, at different irradiation times, were centrifuged twice at 6000 rpm for 15 min to remove the photocatalyst, and the supernatant submitted to the HPLC analysis.

For the study of the recyclability of the heterogeneous photocatalysts, they were recovered as follows: An aqueous mixture of 15 mL containing the four pollutants and Y-NMQ^+ or Y-Mes-Acr-Me^+ was subjected to irradiation as described above. After 46 h, an aliquot was taken to check that the progress of the reaction was as expected. Then, the reaction mixture was centrifuged (8000 rpm for 5 min), the supernatant was removed, and the heterogeneous photocatalyst was washed with 25 mL of clean distilled water for 1 h upon stirring. Then, it was centrifuged again (8000 rpm for 5 min), the supernatant was removed, and the photocatalyst was dried in the oven for 24 h at 100 °C, prior to second use.

The HPLC used for monitoring the progress of the photodegradations was an Agilent 1100 Series model with quaternary pump G1311 A, photodiode detector VWD G1314 A, standard liquid autosampler G1313 A and degasser G1322 A. A Mediterranea Sea 18 column (25 cm × 0.46 cm, 5 μm particle size) was employed. The mobile phase was fixed at $1.5\ mL\ min^{-1}$ with an isocratic mixture of water pH 3 (30%) and acetonitrile (70%). To monitor removal of the pollutants, 100 μL of a ACN:H_2O (4:1) solution of *p*-xylene (3.2×10^{-4} M) were added as internal standard to every sample (500 μL), prior to injection. Then, aliquots of 90 μL from these samples were injected, and detection wavelength was fixed at 215 nm.

2.4. Photophysical instrumentation

A Shimadzu UV-2101PC spectrophotometer was employed to obtain the UV/Vis absorption spectra of the photocatalysts (Figure S1) and the pollutants (Figure S5). Steady-state and time-resolved fluorescence experiments were performed with a Photon Technology International (PTI) LPS-220B spectrofluorometer and with a EasyLife V spectrofluorometer from OBB, respectively. In the case of time-resolved fluorescence, the excitation source was equipped with a pulsed LED (λ_{exc} = 310 nm and 407 nm for NMQ^+ and Mes-Acr-Me^+, respectively); residual excitation signal was filtered in emission by using a cut-off filter (50% transmission at 320 nm and 435 nm for NMQ^+ and Mes-Acr-Me^+, respectively). Monoexponential decay functions that use a deconvolution procedure to separate them from the lamp pulse profile provided the fitted kinetic traces except in the case of NMQ^+ with OPP in which the decay function was fitted to a biexponential relationship. A pulsed Nd: YAG SL404G-10 Spectron Laser Systems at the excitation wavelength of 355 nm was employed to carry out the laser flash photolysis (LFP) experiments. The energy of the single pulses (~10 ns duration) was lower than $15\ mJ\ pulse^{-1}$. The laser flash photolysis system consists of the pulsed laser, a pulsed Lo255 Oriel Xenon lamp, a 77,200 Oriel monochromator, an Oriel photomultiplier tube (PMT) housing, a 70,705 PMT power supply and a TDS-640 A Tektronix oscilloscope.

Photophysical measurements were run in solution (ACN:H_2O, 4:1, for the UV spectra experiments and in ACN and for the fluorescence and LFP experiments), at room temperature, under nitrogen, using quartz cells of 1 cm optical path length. For the fluorescence quenching experiments, solutions of each photocatalyst with absorbance lower than 0.15 at λ_{exc} = 317 nm and 310 nm for NMQ^+ (steady-state and time-resolved, respectively), or 407 nm for Mes-Acr-Me^+, were treated with increasing concentrations of pollutant, up to 5.8 mM, 5.5 mM, 6.1 mM and 4.6 mM for P, OPP, TCP and PCP, respectively. For the LFP experiments, solutions of Mes-Acr-Me^+ with absorbance lower than 0.3 at λ_{exc} = 350 nm, were treated in the absence and in the presence of

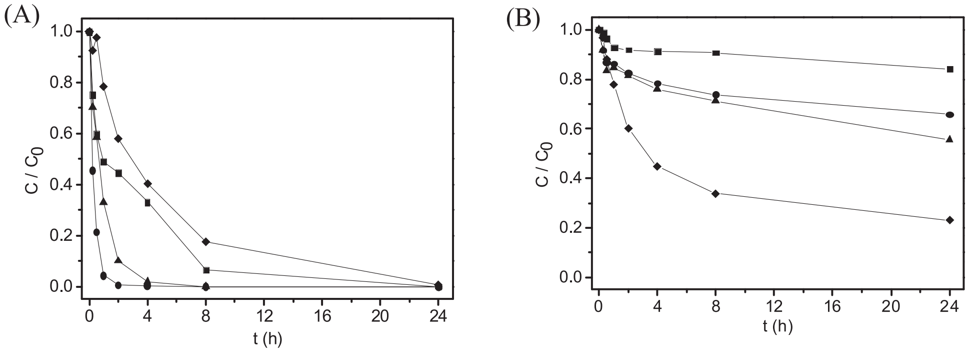

Fig. 3. Plot of the relative concentration of P (■), OPP (●), TCP (▲) and PCP (◆) at initial global concentration of $C_0 = 2 \times 10^{-4}$ M *vs* 350 nm irradiation time in the presence of 20% mol NMQ$^+$ (A) or 420 nm irradiation in the presence of 20% mol Mes-Acr-Me$^+$ (B) under aerated atmosphere in aqueous media.

pollutants, up to 1 mM.

Diffuse reflectance of heterogeneous Y-NMQ$^+$ and Y-Mes-Acr-Me$^+$ were recorded using a Cary 5000 from Agilent Technologies (Figure S6).

3. Results

3.1. Homogeneous photochemical degradations

First, homogeneous photodegradation of aerobic aqueous mixtures of the four pollutants (P, OPP, TCP and PCP) in the presence of different molar ratios of each photocatalyst (5, 10 and 20% mol) was evaluated for 24 h. Irradiation sources were centered at 350 nm or 420 nm, when using NMQ$^+$ or Mes-Acr-Me$^+$, respectively (Figs. 3, S7 and S8). In both cases, the highest level of photodegradation was achieved when photocatalyst was employed at 20% mol, being NMQ$^+$ more efficient than Mes-Acr-Me$^+$, at every molar ratio. Specifically, with NMQ$^+$, removal of the pollutants was completed within 24 h of irradiation. Even more, after 8 h of irradiation, high levels of removal were already achieved (93%, 100%, 100% and 82% for P, OPP, TCP and PCP, respectively), which suggests that irradiation time could be shortened from 24 to 8 h. Yet, Mes-Acr-Me$^+$ was not as effective, and best results were obtained using 20% mol upon 24 h of irradiation. Under these conditions, removal of PCP was 88%, while TCP was 45%, OPP 35% and P resulted in the most recalcitrant contaminant with only 16% of removal. From the irradiation mixtures, no clear-cut peaks were found in the HPLC analysis in any case, pointing out that under these conditions the pollutants disappear giving probably rise to a complex mixture of minor photoproducts, with insufficient individual concentrations to be detected.

Control experiments performed in the absence of light showed that the pollutants remain stable after equivalent reaction periods (results not shown). Those carried out in order to check direct photolysis revealed that at 350 nm irradiation, direct absorption of light is partially responsible for the observed photodegradation, since it produced removal of PCP (up to 50%), P (40%), OPP (20%) and TCP (20%) (Figure S9). Conversely, at 420 nm direct photolysis was marginal, in agreement with the UV spectra of the pollutants (Figure S5). Moreover, the stability of both photocatalysts was also monitored by UV absorption spectra (Figure S10). After 24 h of irradiation, the absorption spectrum of NMQ$^+$ still contained the main bands, although their intensity decreased about 15%, whereas for the case of Mes-Acr-Me$^+$ a significant degradation was observed (about 60%), in agreement with previous reports [20,21].

Therefore, the higher efficiency of NMQ$^+$ to produce the photodegradation of the mixture of pollutants is not only due to its higher redox potential compared to Mes-Acr-Me$^+$, but also to its higher photostability.

3.2. Heterogeneous photochemical degradations

A typical strategy to improve the photostability and easy recovery of the photocatalysts that at the same time increases their potential for future applications involves heterogeneization, most commonly based on the adsorption of the organic compound onto a solid inert material, such as a zeolite [22–25]. For this purpose, NMQ$^+$ and Mes-Acr-Me$^+$ were separately supported onto an inert inorganic support (zeolite Y 100), elemental analysis of the new materials (Y-NMQ$^+$ and Y-Mes-Acr-Me$^+$) revealed a loading of *ca.* 13% and 15% weight for NMQ$^+$ and Mes-Acr-Me$^+$, respectively. Moreover, diffuse reflectance demonstrated the incorporation of the photocatalysts onto the zeolites as evidenced by the presence of the typical chromophores absorption (Figure S6).

Next, to evaluate the performance of Y-NMQ$^+$ and Y-Mes-Acr-Me$^+$, mixtures of the pollutants (5×10^{-5} M each) in aerobic aqueous media, were irradiated using 350 nm or 420 nm centered light in the presence of Y-NMQ$^+$ (26% mol) or Y-Mes-Acr-Me$^+$ (30% mol), respectively (Fig. 4). In the case of Y-NMQ$^+$, the extent of removal was lower than the one achieved in the homogeneous photodegradations for all the pollutants, even with longer irradiation times, except in the case of PCP, whose photodegradation was fully achieved after 30 h. Lower abatement yields have been reported upon heterogeneization of organic photocatalysts, and have been attributed to the more difficult diffusion of the pollutants through the channels of the supports [18]. On the contrary, for the case of Y-Mes-Acr-Me$^+$, heterogeneization resulted in better performance, thus within 46 h irradiation, abatement levels

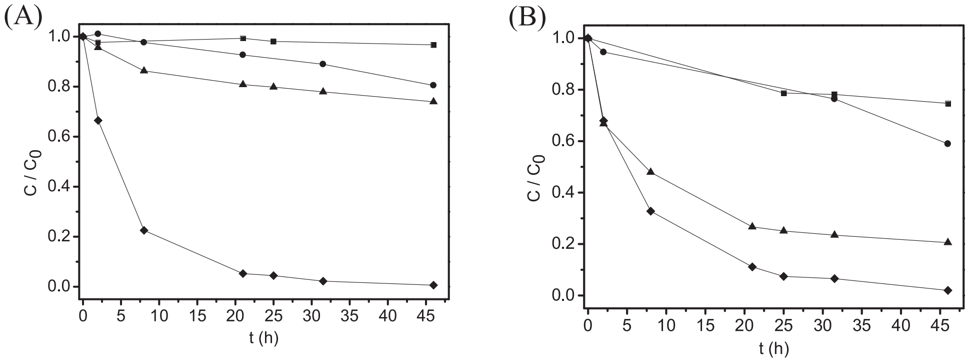

Fig. 4. Plot of the relative concentration of P (■), OPP (●), TCP (▲) and PCP (◆) at initial global concentration of $C_0 = 2 \times 10^{-4}$ M *vs* irradiation time in aerated aqueous media, upon irradiation at 350 nm in the presence of Y-NMQ$^+$ (26% mol) (A) and at 420 nm in the presence of Y-Mes-Acr-Me$^+$ (30% mol) (B).

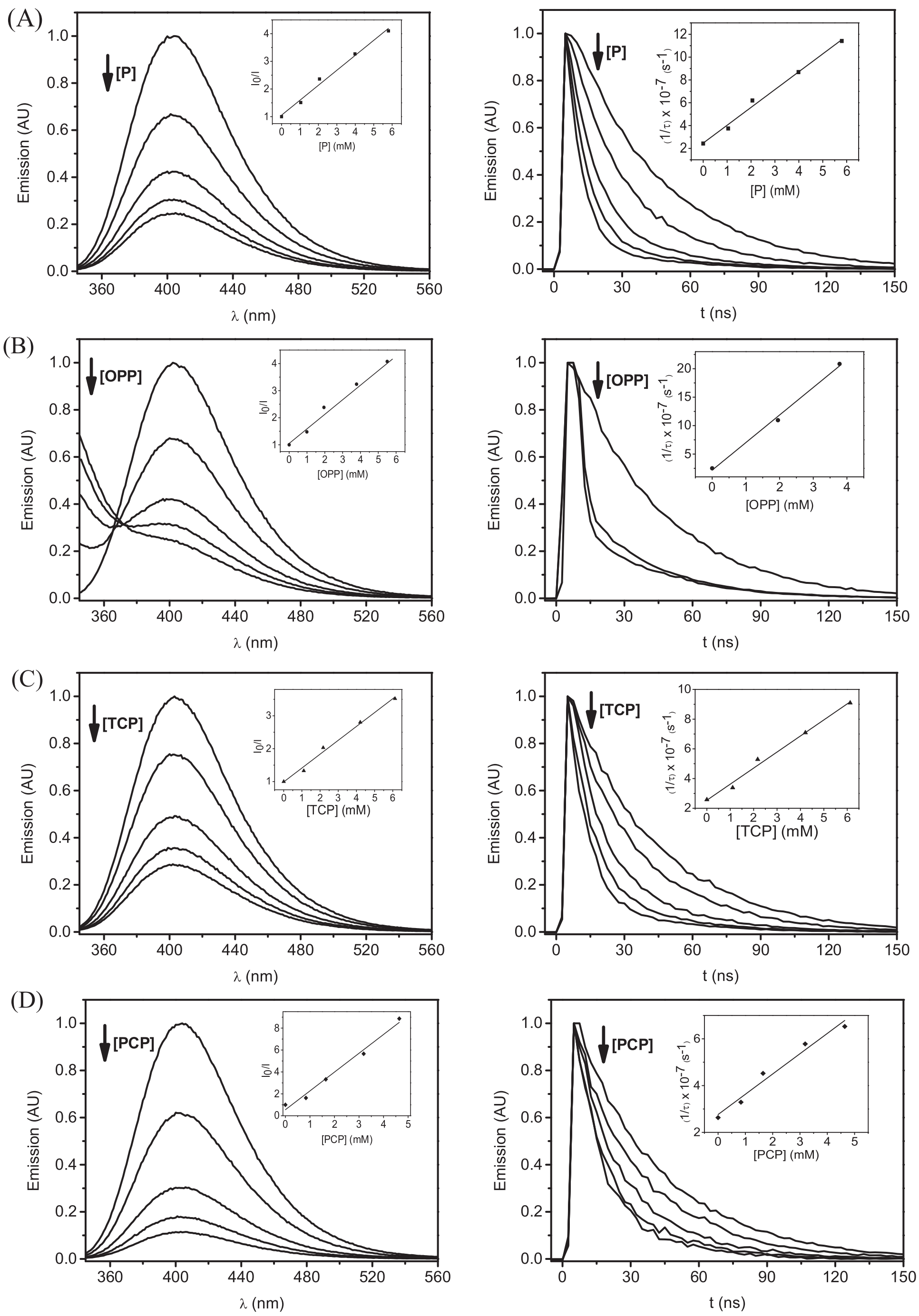

Fig. 5. Steady-state (left column) and time-resolved (right column) $^1(NMQ^+)^*$ fluorescence quenching upon addition of increasing concentrations of P (A), OPP (B), TCP (C) and PCP (D) in ACN under N_2; λ_{exc} = 310 nm. Insets: Stern Volmer plots obtained from the corresponding steady-state (left) and time-resolved (right) experiments.

achieved were 98%, 80%, 40% and 26% for PCP, TCP, OPP and P, respectively, demonstrating the potential of heterogeneous Y-Mes-Acr-Me$^+$ as a visible light photocatalyst. Control experiments to check the adsorption of the pollutants onto the zeolites Y-NMQ$^+$ and Y-Mes-Acr-Me$^+$ indicated that adsorption was lower than 5%, therefore the observed photodegradation was safely attributed to the photocatalyzed degradation. Thus, the better performance of Y-Mes-Acr-Me$^+$ upon incorporation into the zeolite could be attributed to the prevention of nucleophilic attack resulting in lower percentage of photobleaching [10,19].

Accordingly, successful results were obtained for recycled Y-Mes-Acr-Me$^+$: 77%, 29%, 39% and 23% for PCP, TCP, OPP and P, respectively, of abatement accomplished in the second use (see figure S11).

3.3. Involvement of singlet excited species

Steady-state and time resolved fluorescence measurements were carried out in order to determine the participation of the singlet excited state of the photocatalysts in the removal of the contaminants, see Figs. 5 and 6. From these experiments it is clear that every pollutant is able to quench the singlet excited state of both $^1(NMQ^+)^*$ and $^1(Mes\text{-}Acr\text{-}Me^+)^*$. Special attention is required to the case of the quenching of $^1(NMQ^+)^*$ by OPP (Fig. 5B left). The new band observed upon addition

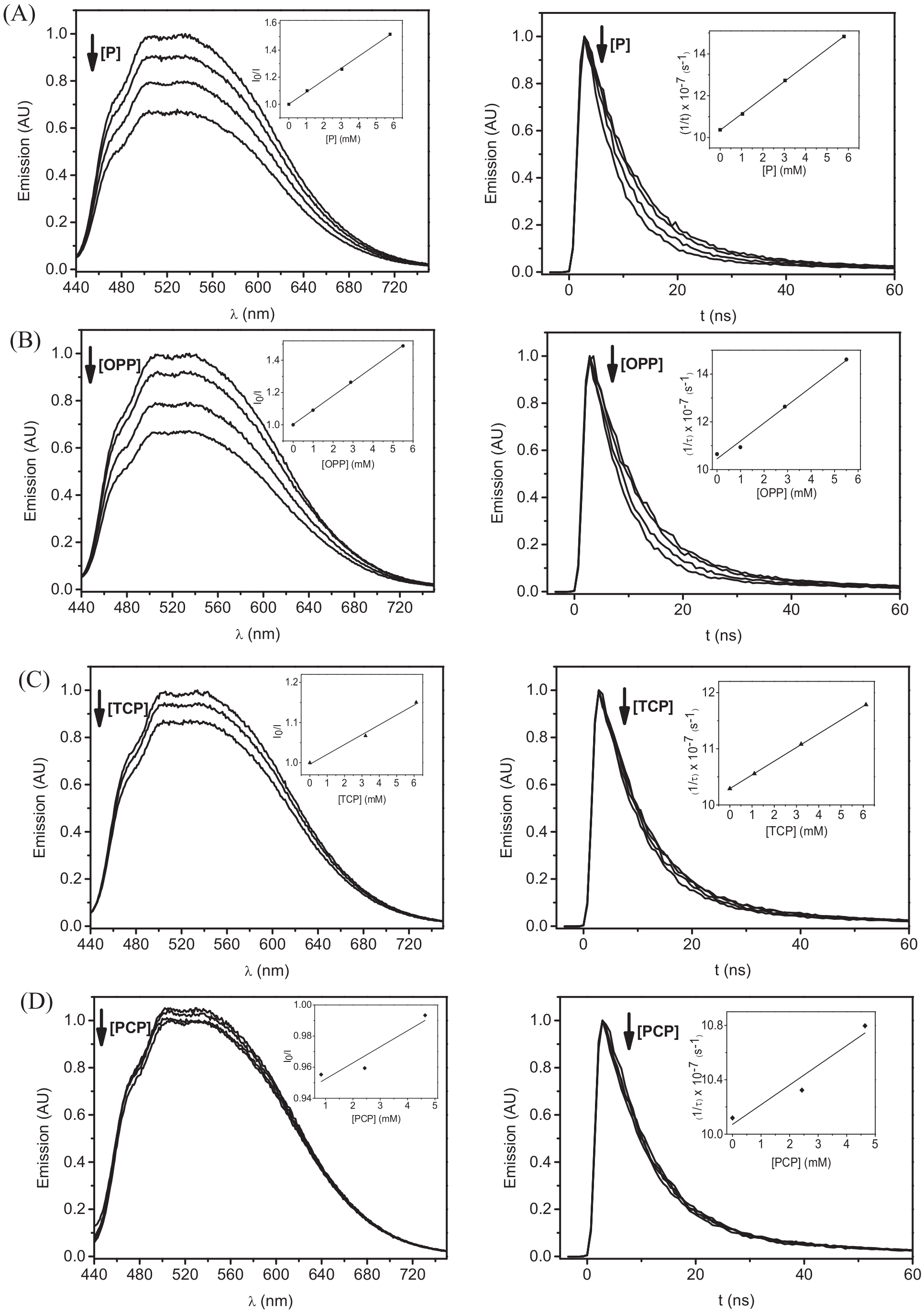

Fig. 6. Steady-state (left column) and time-resolved (right column) $^1(\text{Mes-Acr-Me}^+)^*$ fluorescence quenching upon addition of increasing concentrations of P (A), OPP (B), TCP (C) and PCP (D) in ACN under N_2; λ_{exc} = 310 nm. Insets: Stern Volmer plots obtained from the corresponding steady-state (left) and time-resolved (right) experiments.

Table 1
Rate constant values for the reaction between the pollutants and NMQ^+ and Mes-Acr-Me^+ obtained from steady-state and time-resolved experiments.

	k_q ($M^{-1}s^{-1}$)			
	$^1(NMQ^+)^*$ steady-state	$^1(NMQ^+)^*$ time-resolved	$^1(\text{Mes-Acr-Me}^+)^*$ steady-state	$^3(\text{Mes-Acr-Me}^+)^*$ time-resolved
P	2.7×10^{10}	1.6×10^{10}	1.5×10^{10}	7.7×10^9
OPP	2.7×10^{10}	4.8×10^{10}	1.5×10^{10}	7.5×10^9
TCP	2.1×10^{10}	1.1×10^{10}	4.1×10^9	2.4×10^9
PCP	8.6×10^{10}	8.7×10^9	5.2×10^8	1.4×10^9

of OPP corresponds to the emission of OPP, obtained from the partial direct excitation of OPP at 317 nm. Therefore, the time-resolved measurements required a two-exponential fitting for the decay (see Fig. 5B right). Table 1 reveals an efficient kinetic quenching constants between the pollutants and the singlet excited states of both photocatalysts, with values close to the diffusion limit (in the order of 10^{10} $M^{-1}s^{-1}$) [26].

3.4. Involvement of triplet excited species

Next step was the evaluation of the involvement of the triplet excited species of the photocatalysts in the photodegradations. NMQ^+ is a special photocatalyst as previously described: it exhibits a long lifetime

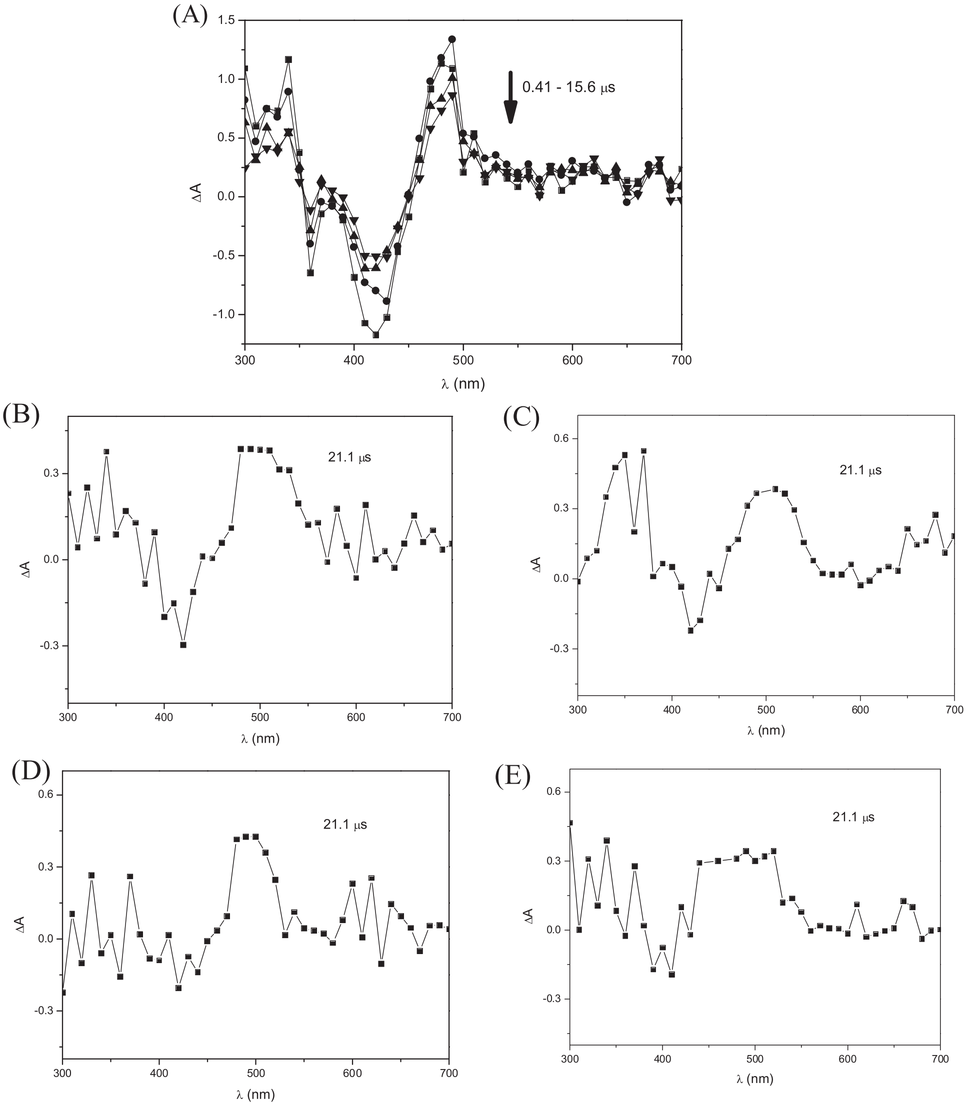

Fig. 7. Transient absorption spectra obtained upon laser flash photolysis excitation in deaerated $CH_3CN:H_2O$ (4:1) (Abs = 0.3 at 355 nm) in the absence (A) or in the presence of 1 mM of the pollutants: P (B), OPP (C), TCP (D) and PCP (E).

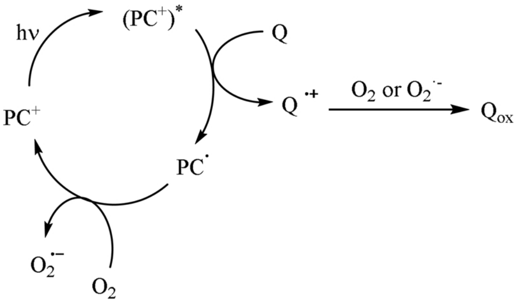

Scheme 1. Photoredox catalytic cycle of NMQ^+ and Mes-Acr-Me^+ (represented as PC^+) involving photooxidation of the pollutants (Q).

Table 2
Estimated free energy changes for the photoinduced electron transfer from the pollutants to the singlet excited state of each photocatalyst, calculated according to Eq. (1).

Pollutant	ΔG^o_{et} NMQ^+ (eV)	ΔG^o_{et} Mes-Acr-Me^+ (eV)
P	−2.04	−1.52
OPP	−1.55	−1.03
TCP	−1.57	−1.05
PCP	−1.03	−0.51

of its singlet excited state and a high fluorescence quantum yield [6,17]. This fact together with the high values of the kinetic constants obtained from the fluorescence experiments, points out an efficient quenching from the singlet, which accordingly, prevents formation of the triplet at the pollutants concentration employed for the photophysical experiments. On the contrary, for the case of Mes-Acr-Me^+, which exhibits lower kinetic constant values for the singlet excited state quenching, laser flash photolysis experiments were performed to investigate the participation of the triplet in the photodegradation. First, the transient spectrum of Mes-Acr-Me^+ was obtained (Fig. 7A), where the corresponding band located at 450–500 nm can be observed (attributed to the local or charge transfer triplet species) [9–11]. Next, the spectrum of the photocatalyst in the presence of each one of the pollutants was obtained (Fig. 7B-E), revealing the formation of the reduced radical species of the photocatalyst [9,11], and, therefore, providing evidence of the redox processes. However, kinetic analysis of the participation of the triplet in the photodegradations was difficult due to the overlap of the triplet and radical signals (Fig. 7).

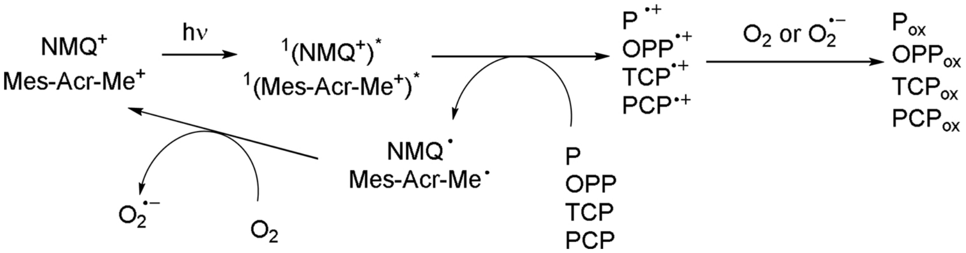

Scheme 2. Potential mechanistic pathway to explain the photooxidation of the pollutants.

3.5. *Thermodynamic feasibility of the redox processes*

As mentioned above, although NMQ^+ and Mes-Acr-Me^+ are able to generate singlet oxygen [11,12], photoinduced electron transfer or the generated superoxide anion must be responsible for the observed photodegradations at the employed pollutant concentration (Scheme 1) [27,28]. Nevertheless, a thermodynamic analysis of the potential participation of the singlet excited state of the photocatalysts can be performed using the photoinduced Gibbs free energy Eq. (1) [29], the experimentally measured redox potentials values (Figure S4, and table S1) and the energy of the excited states (Fig. 2).

$$\Delta G^o_{et} = -\left[E^o_{red}\left(PC^+/PC^\cdot\right) - E^o_{red}\left(Q^{\cdot+}/Q\right)\right] - E^*_{PC^+} \quad (1)$$

where PC^+ represents NMQ^+ and Mes-Acr-Me^+ and Q is any pollutant.

Table 2 reveals that photooxidative degradations are exergonic for both photocatalysts acting from their singlet excited states. To close the photocatalytic cycle, formation of superoxide anion from the reduction of O_2 (E^o_{red} = -0.33 V *vs* SCE) [30] would be exergonic in both cases (-0.52 eV and -0.16 eV for NMQ^+ and Mes-Acr-Me^+, respectively) [27,28].

The obtained values reveal that, as expected, singlet excited states of both photocatalysts could, in principle, participate in the photoinduced electron transfer. Nevertheless, it is mandatory to perform kinetic studies to evaluate the viability of the electron transfer in the time scale of those excited states.

3.6. *Mechanistic proposal*

Scheme 2 shows the postulated mechanism to explain photooxidation of the phenolic pollutants. Quenching of the singlet excited states resulted to be dynamic acting as a proof of the participation of these excited states in the photoinduced electron transfer. Thus, Type I photooxidation happening through the singlet excited state of either photocatalyst is the main operating process in the photodegradation of the studied pollutants, although participation of the triplet cannot be precluded.

4. Conclusions

Homogeneous photodegradation of phenolic compounds can be efficiently achieved with both photocatalysts, NMQ^+ and Mes-Acr.-Me^+; however, the rate of the process depends on the nature of the photocatalyst. Thus, the highly oxidizing NMQ^+ leads to higher degradation levels, which in part is due to direct photolysis. In the case of Mes-Acr-Me^+, its lower redox potential and photostability results in a reduced photoactivity and therefore in a slower degradation; however, its capability to absorb visible light may be advantageous for environmental applications. After heterogenization, the stability of Mes-Acr-Me^+ increases and the removal of the pollutants becomes more efficient. Steady-state and time resolved fluorescence quenching reveal that both photocatalysts are capable of oxidizing the pollutants from their singlet excited states, with kinetic rate constants in the order of the diffusion limit.

Acknowledgements

Financial support from Spanish Government (Grant SEV-2016-0683) is gratefully acknowledged. Financial support from VLC/Campus. R. Martinez-Haya thanks financial support for a predoctoral contract from Apadrina la Ciencia Association and Ford España/Ford Motor Company Fund.

Appendix A. Supplementary data

Supplementary data associated with this article can be found, in the online version, at https://doi.org/10.1016/j.cattod.2019.01.045.

References

[1] G. Banias, C. Achillas, C. Vlachokostas, N. Moussiopoulos, M. Stefanou, Environmental impacts in the life cycle of olive oil: a literature review, J. Sci. Food Agric. 97 (2017) 1686–1697.
[2] M. Beccari, F. Bonemazzi, M. Majone, C. Riccardi, Interaction between acidogenesis and methanogenesis in the anaerobic treatment of olive oil mill effluents, Water Res. 30 (1996) 183–189.
[3] N. Adhoum, L. Monser, Decolourization and removal of phenolic compounds from olive mill wastewater by electrocoagulation, Chem. Eng. Process. Process. Intensif. 43 (2004) 1281–1287.
[4] C. Amor, M.S. Lucas, J. García, J.R. Dominguez, J.B. De Heredia, J.A. Peres, Combined treatment of olive mill wastewater by Fenton's reagent and anaerobic biological process, J. Environ. Sci. Health 50 (Part A) (2015) 161–168.
[5] S. Malato, P. Fernandez-Ibanez, M.I. Maldonado, J. Blanco, W. Gernjak, Decontamination and disinfection of water by solar photocatalysis: Recent overview and trends, Catal. Today 147 (2009) 1–59.
[6] M.L. Marin, L. Santos-Juanes, A. Arques, A.M. Amat, M.A. Miranda, Organic photocatalysts for the oxidation of pollutants and model compounds, Chem. Rev. 112 (2012) 1710–1750.
[7] M.A. Miranda, F. Galindo, A.M. Amat, A. Arques, Pyrylium salt-photosensitised degradation of phenolic contaminants present in olive oil wastewaters with solar light: Part II. Benzoic acid derivatives, Appl. Catal. B 30 (2001) 437–444.
[8] S. Fukuzumi, H. Kotani, K. Ohkubo, S. Ogo, N.V. Tkachenko, H. Lemmetyinen, Electron-transfer state of 9-mesityl-10-methylacridinium ion with a much longer lifetime and higher energy than that of the natural photosynthetic reaction center, J. Am. Chem. Soc. 126 (2004) 1600–1601.
[9] N.A. Romero, D.A. Nicewicz, Mechanistic Insight into the Photoredox Catalysis of Anti-Markovnikov Alkene Hydrofunctionalization Reactions, J. Am. Chem. Soc. 136 (2014) 17024–17035.
[10] S. Fukuzumi, K. Ohkubo, T. Suenobu, Long-lived charge separation and applications in artificial photosynthesis, Acc. Chem. Res. 47 (2014) 1455–1464.
[11] A.C. Benniston, A. Harriman, P. Li, J.P. Rostron, H.J. van Ramesdonk, M.M. Groeneveld, H. Zhang, J.W. Verhoeven, Charge shift and triplet state formation in the 9-mesityl-10-methylacridinium cation, J. Am. Chem. Soc. 127 (2005) 16054–16064.
[12] R. Martinez-Haya, C. Sabater, M.-Á. Castillo, M.A. Miranda, M.L. Marin, A mechanistic study on the potential of quinolinium salts as photocatalysts for the abatement of chlorinated pollutants, J. Hazard. Mater. 351 (2018) 277–284.
[13] R. Martinez-Haya, M.A. Miranda, M.L. Marin, Type I vs Type II photodegradation of pollutants, Catal. Today 313 (2018) 161–166.
[14] H. Kotani, K. Ohkubo, S. Fukuzumi, Photocatalytic oxygenation of anthracenes and olefins with dioxygen via selective radical coupling using 9-mesityl-10-methylacridinium ion as an effective electron-transfer photocatalyst, J. Am. Chem. Soc. 126 (2004) 15999–16006.
[15] H. Kotani, K. Ohkubo, S. Fukuzumi, Formation of hydrogen peroxide from coal tar as hydrogen sources using 9-mesityl-10-methylacridinium ion as an effective photocatalyst, Appl. Catal. B 77 (2008) 317–324.
[16] P.F. Donovan, D.A. Conley, Some organic tetrafluoroborates, J. Chem. Eng. Data 11 (1966) 614-&.
[17] U.C. Yoon, S.L. Quillen, P.S. Mariano, R. Swanson, J.L. Stavinoha, E. Bay, Exploratory and mechanistic aspects of the electron-transfer photochemistry of olefin-N-heteroaromatic cation systems, J. Am. Chem. Soc. 105 (1983) 1204–1218.

[18] A. Arques, A.M. Amat, L. Santos-Juanes, R.F. Vercher, M.L. Marin, M.A. Miranda, Abatement of methidathion and carbaryl from aqueous solutions using organic photocatalysts, Catal. Today 144 (2009) 106–111.

[19] S. Fukuzumi, K. Doi, A. Itoh, T. Suenobu, K. Ohkubo, Y. Yamada, K.D. Karlin, Formation of a long-lived electron-transfer state in mesoporous silica-alumina composites enhances photocatalytic oxygenation reactivity, Proc. Natl. Acad. Sci. 109 (2012) 15572–15577.

[20] T. Hering, T. Slanina, A. Hancock, U. Wille, B. König, Visible light photooxidation of nitrate: the dawn of a nocturnal radical, Chem. Commun. 51 (2015) 6568–6571.

[21] A.C. Benniston, K.J. Elliott, R.W. Harrington, W. Clegg, On the photochemical stability of the 9-Mesityl-10-methylacridinium cation, European J. Org. Chem. 2009 (2009) 253–258.

[22] V. Ramamurthy, J.V. Caspar, D.R. Corbin, Generation, entrapment, and spectroscopic characterization of radical cations of. alpha.,.omega.-diphenyl polyenes within the channels of pentasil zeolites, J. Am. Chem. Soc. 113 (1991) 594–600.

[23] F. Gessner, J.C. Scaiano, Intrazeolite photochemistry VII: Laser photolysis of stilbene and some aromatic hydrocarbons in the cavities of NaX zeolite studied by time-resolved diffuse reflectance, J. Photochem. Photobiol. A: Chem. 67 (1992) 91–100.

[24] S. Sankararaman, K.B. Yoon, T. Yabe, J.K. Kochi, Control of back electron transfer from charge-transfer ion pairs by zeolite supercages, J. Am. Chem. Soc. 113 (1991) 1419–1421.

[25] A.M. Amat, A. Arques, S.H. Bossmann, A.M. Braun, S. Gob, M.A. Miranda, A "Camel through the eye of a needle": direct introduction of the TPP+ ion inside Y-zeolites by formal ion exchange in aqueous medium, Angew. Chem., Int. Ed. 42 (2003) 1653–1655.

[26] S.L. Murov, I. Carmichael, G.L. Hug, Handbook of Photochemistry, 2nd ed., Marcel Dekker, New York, 2009.

[27] H. Huang, A.H. Reshak, S. Auluck, S. Jin, N. Tian, Y. Guo, Y. Zhang, Visible-light-responsive sillén-structured mixed-cationic CdBiO2Br nanosheets: layer structure design promoting charge separation and oxygen activation reactions, J. Phys. Chem. C 122 (2018) 2661–2672.

[28] H. Huang, S. Tu, C. Zeng, T. Zhang, A.H. Reshak, Y. Zhang, Macroscopic polarization enhancement promoting photo- and piezoelectric-induced charge separation and molecular oxygen activation, Angew. Chem. Int. Ed. 56 (2017) 11860–11864.

[29] D. Rehm, A. Weller, Kinetics of fluorescence quenching by electron and H-atom transfer, Isr. J. Chem. 8 (1970) 259–271.

[30] Y.A. Ilan, D. Meisel, G. Czapski, The redox potential of the O2–O − 2 system in aqueous media, Isr. J. Chem. 12 (1974) 891–895.